

Influence of spherical anisotropy on optical mass sensing in a molecular-plasmonic optomechanical system

Elnaz Alebrahim,¹ Malek Bagheri Harouni,^{1,2,*} and Ehsan Amooghorban^{3,4,†}

¹*Department of Physics, University of Isfahan, Hezar Jerib St., Isfahan 81764-73441, Iran.*

²*Quantum optics group, Department of Physics, University of Isfahan, Hezar Jerib St., Isfahan 81764-73441, Iran.*

³*Department of Physics, Faculty of Basic Sciences,*

Shahrekord University, P.O. Box 115, Shahrekord 88186-34141, Iran.

⁴*Photonic Research Group, Shahrekord University, Shahrekord 88186-34141, Iran.*

We use an all-optical pump-probe method to develop a mass sensing mechanism in a molecular plasmonic system at room temperature. The system consists of a double-clamped graphene nanoribbon that parametrically interacts with two types of isotropic and anisotropic spherical plasmonic cavities in the presence of a strong pump field and a weak probe pulse. Based on the mode-selective quantization scheme and analogy with the canonical model of the cavity optomechanics, we formulate the Hamiltonian of the system in terms of the electromagnetic Green's tensor. In this manner, we derive an explicit form of size-dependent optomechanical coupling function and plasmonic damping rate, which include the modal, geometrical, and material features of the plasmonic structure. Engineering material features of the plasmonic nanostructure, we find that the intensity of the probe field transmission spectrum for radially anisotropic spherical nanocavity enhances significantly compared to the silver sphere nanocavity due to the mode volume reduction. This scheme can provide to achieve the minimum measurable mass $\Delta m \approx 10^{-24} kg$ at room temperature.

I. INTRODUCTION

One of the most promising methods for tailoring light-matter interaction is to employ metallic structures in nanoscale size as plasmonic nanocavities [1–6]. Localized plasmon resonances (LPR), which result from the confinement of light waves within the metallic subwavelength structures, are considered as the fundamental concept of a new growing field known as plasmonic cavity quantum electrodynamics (PCQED) [7–9]. These localized plasmons can be effectively controlled by adjusting cavity composition, size, shape, and the material parameters of the surrounding medium. The sub-diffraction-limit focusing of electromagnetic fields in the near-field of the LPRs is responsible for the enormous enhancement of the Raman spectrum in a commonly sensing technique known as the surface-enhanced Raman scattering (SERS) [10]. So far, the dynamical behavior of SERS phenomena, which represents the interaction between molecular species and metallic nanoparticles, was formulated theoretically in the field of molecular plasmonic in both classical and quantum regimes [1, 3, 5, 11]. Many attempts have been devoted to investigate the influence of material and geometrical parameters such as anisotropy on the SERS enhancement factor by finding the scalar potential distribution of the nanostructure and extracting its polarizability in the quasi-static approximation (QSA) [12].

Recently a theoretical approach is introduced to explain the dynamical nature of plasmon-phonon interaction by mapping the molecular plasmonic system onto

the canonical model of cavity optomechanics [13]. Based on this model, it is shown that the polarizability of the molecule and its interaction with a plasmonic nanocavity are explicitly dependent on the internal vibrational states of the adjacent molecule [14, 15]. This theoretical approach was applied to the SERS phenomenon and successfully described fundamental classical properties such as the dependence of the Raman signal on the intensity and frequency of the incident laser. Quantum features like dynamical back-action amplification, which are related to the vibrational modes and correlations between emitted photons of the molecules, can be described through the molecular optomechanical model [14–17].

Several challenging phenomena such as distinguishing similar molecules and designing tunable optical switches have been studied in this framework [18]. Heat transfer of two adjacent molecules in a plasmonic nanocavity, optomechanical cooling in the nonlinear regime, collective effects in SERS, and optical mass sensing are other noticeable phenomena that have recently been investigated through this optomechanical model [12, 18–21].

Liu et al. proposed recently a mass sensing setup with high precision at room temperature using an artificial molecule with a small effective mass instead of a real Raman active molecule in the vicinity of plasmonic nanostructures [22]. It is an interesting mass sensing system due to the large mass sensitivity of the mechanical resonator resulting from the large plasmon-phonon coupling [22–24].

The canonical model of cavity optomechanics can provide the ability to analyze the molecular plasmonic systems and subsequently investigate the effects of several parameters such as incident pump field, coupling strength, and plasmonic damping rate on the transmission spectrum. However, the explicit dependence of these parameters upon the material and geometrical features of

* Corresponding author: m-bagheri@phys.ui.ac.ir

† Corresponding author: Ehsan.amooghorban@sku.ac.ir

the system has been studied less analytically [25]. Establishing a formalism that prepares the physical ground to understand the influences of these parameters on the dynamics of the system and control the transmission peak height and shape of the probe beam, would be practically useful. Therefore, as the main purpose of this study, we intend to enter these features into the optomechanical formalism of the molecular plasmonic system.

Unlike the traditional method based on the first-principle approach to obtain polarizability of plasmonic nanostructure for sensing purpose [12], in the present contribution, we start with the mode-selective quantization scheme to extract the optomechanical Hamiltonian describing the interaction between a plasmonic nanostructure and a suspended graphene nanoribbon (SGNR) [26, 27]. This Hamiltonian contains the electromagnetic Green's tensor of the system through which dispersive and dissipative properties of plasmonic cavities enter into the formalism. We then focus on two types of isotropic and anisotropic spherical plasmonic cavities and derive the multipolar polarizability from the Green's tensor of the system in the quasi-static approximation. In this way, we can analytically derive the optomechanical coupling strength, which includes the modal volume of the plasmonic subsystem. The modal volume is a crucial concept in the field of PCQED that quantifies the magnitude of the electric field confinement. Although this parameter is not the geometrical volume but depends on the geometrical properties of the nanocavities [28, 29].

This paper is organized as follows. In section II, we present the details of the mode-selective quantization method and then generalize this theoretical treatment to formulate a multimode optomechanical Hamiltonian expressing the interaction between plasmonic nanostructures and the SGNR. To further illustrate the flexibility of this method, in section III we determine the explicit expression of the optomechanical strength and modal volume for coupling of the isotropic and anisotropic spherical plasmonic cavities with the SGNR. We subsequently obtain the transmission spectrum of the probe field related to the two aforementioned plasmonic systems for the sensing process at room temperature. In section IV, numerical results associated with the spectral function, optomechanical strength, and transmission spectrum are depicted and discussed. The paper is summarized by exploring optimal mass sensing in section V. Details related to the mode-selective quantization, the quantum Langevin equations, and the Mie coefficients can be found in Appendices A to D, respectively.

II. THEORETICAL FRAMEWORK

Consider a system (Fig. 1) composed of a double clamped graphene nanoribbon in the vicinity of a spherical plasmonic nanocavity with radius R in the presence of external fields. The graphene nanoribbon lies in the xy plane, and its axis direction is along y . We suppose that

the nanoribbon is located at the equilibrium distance r_m from the center of the spherical cavity at origin and can vibrate in horizontal direction. Here, the nanoribbon vibrations associated with the breathing-like mode, where all the atoms of the nanoribbon move in-plane along the ribbon width direction, as shown in Fig. 1. This mode is Raman active due to the inversion symmetry of the atoms-displacement pattern in the nanoribbon [30]. We can well characterize the vibrational mode of the SGNR by a harmonic oscillator with frequency ω_m . The relative permittivity of the background medium is taken to be that of free space, $\epsilon_1 = 1$, and $\bar{\epsilon}$ is the relative permittivity tensor of the spherical nanocavity.

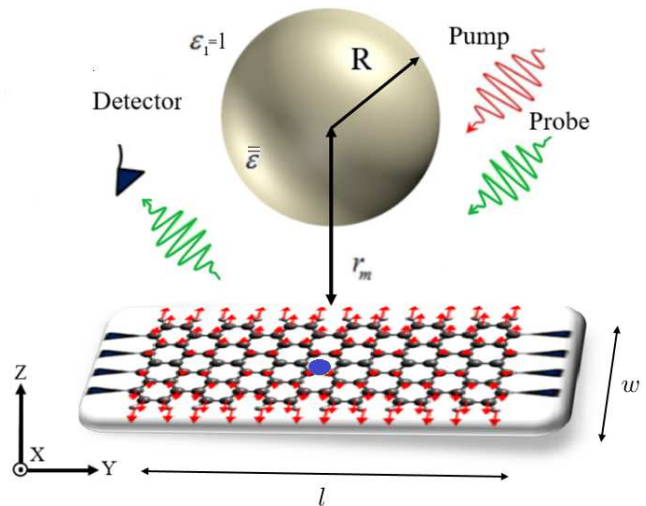


FIG. 1: (a) A schematic representation of the parametric interaction between the plasmonic cavity mode and suspended graphene nanoribbon in the presence of a strong pump field and a weak probe field. Here, plasmonic nanostructure is placed in vacuum. Double clamped graphene nanoribbon (armchair configuration) is located in the xy plane with periodicity direction along y .

Free Hamiltonian of the whole system is given by $\hat{H}_{free} = \hat{H}_m + \hat{H}_p$, in which the first term refers to the mechanical vibrations of the SGNR, i.e. $\hat{H}_m = \hbar\omega_m \hat{b}^\dagger \hat{b}$. Here, \hat{b}^\dagger (\hat{b}) is the creation (annihilation) operator of the vibrational mode of the SGNR with the frequency ω_m . \hat{H}_p is the free Hamiltonian of the plasmonic subsystem and describes the total energy of the electromagnetic field in a lossy plasmonic medium, so it can be written as:

$$\hat{H}_p = \int d^3r \int_0^\infty d\omega \hbar\omega \hat{\mathbf{f}}^\dagger(\mathbf{r}, \omega) \cdot \hat{\mathbf{f}}(\mathbf{r}, \omega), \quad (1)$$

where the bosonic operators $\hat{\mathbf{f}}^\dagger(\mathbf{r}, \omega)$ and $\hat{\mathbf{f}}(\mathbf{r}, \omega)$ represent the collective excitations of the electromagnetic field and the medium with the commutation relation $[\hat{f}_i(\mathbf{r}, \omega), \hat{f}_j^\dagger(\mathbf{r}', \omega')] = \delta_{ij} \delta(\mathbf{r} - \mathbf{r}') \delta(\omega - \omega')$ [31, 32].

Let us theoretically model the parametric coupling between the optical modes of plasmonic structure and the

vibrational mode of the SGNR in the framework of the molecular optomechanics [14]. This interaction Hamiltonian can be described by the dipole interaction:

$$\hat{H}_{int} = -\hat{\mathbf{P}}(\mathbf{r}_m) \cdot \hat{\mathbf{E}}(\mathbf{r}_m). \quad (2)$$

Here, the induced Raman polarization $\hat{\mathbf{P}}(\mathbf{r}_m)$ can be identified with the Raman polarizability tensor of the vibrational mode of the SGNR, $\bar{\alpha}_R$, as $\hat{\mathbf{P}}(\mathbf{r}_m) = -\bar{\alpha}_R \cdot \hat{\mathbf{E}}(\mathbf{r}_m)$. The Raman polarizability can be expressed in terms of the quantized displacement operator of nanoribbon via the relation $\bar{\alpha}_R = -\sqrt{\hbar/2\omega_m}(\hat{b} + \hat{b}^\dagger)\bar{\mathcal{R}}$, wherein the second rank Raman tensor $\bar{\mathcal{R}}$ depends on the molecular structure and bonds nature of the SGNR [13].

Based on the canonical quantization scheme for the electromagnetic field in a dispersive and lossy medium [31–34], the positive frequency part of the electric field operator $\hat{\mathbf{E}}^{(+)}$ can be written as

$$\hat{\mathbf{E}}^{(+)}(\mathbf{r}_m, \omega) = i(\omega^2/c^2) \int d^3r \sqrt{\frac{\hbar \bar{\epsilon}_I(\mathbf{r}, \omega)}{\pi \epsilon_0}} \bar{\mathbf{G}}(\mathbf{r}_m, \mathbf{r}, \omega) \cdot \hat{\mathbf{f}}(\mathbf{r}, \omega), \quad (3)$$

where $\bar{\epsilon}_I(\mathbf{r}, \omega)$ is the imaginary part of the permittivity tensor of medium, and $\bar{\mathbf{G}}(\mathbf{r}_m, \mathbf{r}, \omega)$ is the classical Green's tensor satisfying the Helmholtz equation together with appropriate boundary conditions. The symmetry-related considerations in the point group theory for the graphene nanoribbon [35, 36] along with the method of mode-selective quantization [26] allow us to derive a final discrete form of the Hamiltonian based on the new frequency-independent plasmonic operators $\hat{a}_n(r_m)$ at the position of nanoribbon as

$$\begin{aligned} \hat{H}_{sys} = & \sum_{n=1}^N \hbar\omega_n \hat{a}_n^\dagger(\mathbf{r}_m) \hat{a}_n(\mathbf{r}_m) + \hbar\omega_m \hat{b}^\dagger \hat{b} \\ & - 2\hbar(\hat{b} + \hat{b}^\dagger) \sum_{n=1}^N g_{op,n} \hat{a}_n^\dagger(\mathbf{r}_m) \hat{a}_n(\mathbf{r}_m), \end{aligned} \quad (4)$$

where, ω_n describes the n^{th} resonance frequency of the plasmonic cavity. Furthermore, the frequency-independent coupling function $g_{op,n} = 2|g_n(r_m)|^2$, which is known as optomechanical coupling strength, can be obtained employing the spectral functions through the relation $|g_n(r_m)|^2 = \int d\omega |k_n(r_m, \omega)|^2$. More details on how this optomechanical coupling spectra, $K_n = |k_n(r_m, \omega)|^2$, is generated and also the steps for obtaining this Hamiltonian are outlined in Appendices A and B.

Mass sensing in the pump-probe technique requires examining the probe response of the SGNR [37, 38]. To this purpose, the plasmonic subsystem is coherently driven by a strong pump field and a much weaker probe field, as shown in Fig. 1. Given this, we can obtain the total Hamiltonian of the system only by adding driving terms to the Hamiltonian \hat{H}_{sys} . For more convenience, we recast the total Hamiltonian in a reference frame rotating

at the pump frequency. It yields

$$\begin{aligned} \hat{H}_{tot} = & \hbar\omega_m \hat{b}^\dagger \hat{b} + \sum_{n=1}^N [\hbar\Delta_n \hat{a}_n^\dagger(\mathbf{r}_m) \hat{a}_n(\mathbf{r}_m) \\ & - \hbar g_{op,n} \hat{a}_n^\dagger(\mathbf{r}_m) \hat{a}_n(\mathbf{r}_m) (\hat{b}^\dagger + \hat{b}) \\ & - i\hbar\Omega_{pr} (\hat{a}_n(\mathbf{r}_m) e^{i\delta t} - \hat{a}_n^\dagger(\mathbf{r}_m) e^{-i\delta t}) \\ & - i\hbar\Omega_{pu} (\hat{a}_n(\mathbf{r}_m) - \hat{a}_n^\dagger(\mathbf{r}_m))] , \end{aligned} \quad (5)$$

where Ω_{pu} and Ω_{pr} are coherent driving coupling parameters related to the n^{th} localized surface plasmonic (LSP_n) mode with $\Omega_i = \kappa_n \sqrt{\epsilon_0 V_{eff}} / 2\hbar\omega_n E_{i,m} / 2$ ($i = pu, pr$) [39]. Here, $\kappa_n = \Gamma_n / 2$ and $E_{i,m}$ are the damping rate of LSP_n mode and the maximum near field scattered by the structure, respectively. The $E_{i,m}$ can be written in terms of plasmonic enhancement factor and incident pump field [40]. The parameter $\Delta_n = \omega_n - \omega_{pu}$ denotes the detuning between the pump and the n^{th} mode plasmonic frequency, and the detuning between the probe and pump field is defined as $\delta = \omega_{pr} - \omega_{pu}$.

Using the Heisenberg-Langevin approach [15, 41], which includes dissipation and fluctuation mechanisms in the system, we can determine the time evolution of the plasmonic annihilation operator and the mean response of the mechanical subsystem. Since the incident probe field is much weaker than the pump field, we can employ the perturbation method to investigate the response of the probe field. Appendix C provides the derivation details of output amplitude in the frequency of probe field based on the pump-probe technique and input-output theory. These calculations help us to build the output amplitude $a_{n+,out} = \sqrt{2\kappa_n} a_{n+}$, or equivalently, define the transmission of the probe beam as the ratio of the output and input amplitudes, i.e. $t(\omega_{pr}) = 1 - 2\kappa_n a_{n+} / \Omega_{pr}$ [15]. We will show that the a_{n+} contains all information about optomechanical strength and plasmonic damping rate of the n^{th} plasmonic mode as well as the material and geometrical features, as will be seen in Eq. (C4). Determining the coupling strength in terms of the Green tensor and using the procedure presented in the next section, we would analyze the probe response associated with the several plasmonic subsystems.

III. PLASMONIC CAVITIES

To illustrate how geometrical and material features of plasmonic structure can modify the dynamic of the system and consequently the mass sensing precision, in the present section, we consider two cases and determine the explicit form of the optomechanical strength for them. We then study probe responses in each case.

A. Anisotropic spherical nanostructure optomechanically coupled to the SGNR

In the first case, we consider a uniaxial anisotropic sphere illuminated by a plane wave. The form of the relative permittivity tensor for this anisotropic sphere is given by

$$\bar{\bar{\epsilon}} = \left[(\epsilon_r - \epsilon_t) \hat{\mathbf{r}}\hat{\mathbf{r}} + \epsilon_t \bar{\bar{\mathbf{I}}} \right], \quad (6)$$

where $\bar{\bar{\mathbf{I}}}$ is the unit dyad, and ϵ_r and ϵ_t are the radial and tangential components of the permittivity tensor, respectively [42]. With the general form of Green's tensor in hand and applying the symmetry consideration related to the radial anisotropic sphere, the scattering part of the Green's tensor for the tangential direction is simplified as follows

$$\begin{aligned} \bar{\bar{G}}_{s,tt}^{(11)}(r_m, r_m) &= \frac{i\omega}{8\pi c} \sum_{n=0}^{\infty} (2n+1) \\ &\times \left[B_N^{11} \left(\zeta'_n(k_1 r_m) / k_1 r_m \right)^2 + B_M^{11} \left(h_n^{(1)}(k_1 r_m) \right)^2 \right], \end{aligned} \quad (7)$$

where $k_1 = \omega/c$, $h_n^{(1)}(k_1 r_m)$ is the first-type spherical Hankel function in the position of the nanoribbon, $\zeta_n(k_1 r_m) = (k_1 r_m) h_n^{(1)}(k_1 r_m)$ is the spherical Riccati-Hankel function of the first kind, and the primed function refers to the derivative with respect to its argument. For uniaxial anisotropic sphere with source and field points in the first layer, anisotropy effects appear only in the Mie coefficients $B_l^{(11)} = -T_{l,12}^{(1)}/T_{l,11}^{(1)}$ with $l = N, M$. Here, $T_{l,12}^{(1)}$ and $T_{l,11}^{(1)}$ are the elements of transmission T-matrix that are derived in Appendix D. If the radius of the sphere is very small compared to the wavelength of the incident field, we can restrict our attention to the QSA and simplify the Mie coefficients in this limit [43–45].

As described in Appendix D, the relevant Mie coefficient in our system is $B_N^{(11)}$. It is shown that in the QSA, $B_N^{(11)}$ will be proportional to the modified quasi-static polarizability. This modified polarizability takes exactly the same form of the polarizability as an isotropic sphere if we define an effective permittivity ϵ_{eff}^{ani} as below

$$\epsilon_{eff}^{ani} = \frac{v}{n} \epsilon_r. \quad (8)$$

Here, $v = [n(n+1)AR + 1/4]^{1/2} - 1/2$, in which the anisotropy ratio AR defined as $AR = \epsilon_t/\epsilon_r$ [42]. In what follows, we assume both radial and tangential components of the permittivity tensor in Eq. (8) are given by the Drude-like model $\epsilon_i = \epsilon_{\infty i} - \omega_{pi}^2/\omega(\omega + i\Gamma_{pi})$ with $i = t, r$. We also suppose that the optical parameters of two components obey the relations $\omega_{pr}^2/\epsilon_{\infty r} = \omega_{pt}^2/\epsilon_{\infty t}$ and $\Gamma_{pr} = \Gamma_{pt} = \Gamma_p$. According to these assumptions, the effective permittivity ϵ_{eff}^{ani} takes a Drude-like form,

$\epsilon_{eff}^{ani} = \epsilon_{\infty}^{ani} - (\omega_p^{ani})^2/\omega(\omega + i\Gamma_p)$, in which the optical parameters are defined as follows:

$$\omega_p^{ani} = \left((n(n+1)AR_{\infty}/n^2 + 1/4n^2)^{1/2} - 1/2n \right)^{1/2} \omega_{pr}, \quad (9a)$$

$$\epsilon_{\infty}^{ani} = \left((n(n+1)AR_{\infty}/n^2 + 1/4n^2)^{1/2} - 1/2n \right) \epsilon_{\infty r}. \quad (9b)$$

Here, ω_p^{ani} and ϵ_{∞}^{ani} represent the effective bulk plasmon frequency and the effective high-frequency limit of the dielectric function, respectively. Furthermore, the anisotropy ratio reduces to the constant parameter $AR_{\infty} = \epsilon_{\infty t}/\epsilon_{\infty r}$ [45, 46]. Therefore, we can easily find the approximate imaginary part of the Green tensor in the tangential direction near the resonance frequencies of the plasmonic cavity (for more details refer to Appendix D). Substituting this result into Eq. (A6), we get the approximate expression for the near-field frequency-dependent optomechanical coupling spectra as:

$$\begin{aligned} K_n &\approx \sqrt{\frac{\hbar}{2\omega_m}} \left(\frac{\bar{\mathcal{R}} \omega_n^{ani}}{16\pi\epsilon_0} \right) \frac{n(n+1)(2n+1)R^{2n+1}}{[n\epsilon_{\infty}^{ani} + (n+1)]r_m^{2n+4}} \\ &\times \frac{\Gamma_n^{ani}/2\pi}{(\omega_n^{ani} - \omega)^2 + (\Gamma_n^{ani}/2)^2}. \end{aligned} \quad (10)$$

Here, R , r_m and $\bar{\mathcal{R}}$ represent the radius of the anisotropic sphere, the separation distance of the SGNR from the center of sphere and diagonal elements of the Raman tensor \mathcal{R}_{ii} for $i = x$, respectively. The resonance frequency ω_n^{ani} and the total width Γ_n^{ani} corresponding to the n^{th} localized surface plasmonic mode (LSP_n) of the anisotropic sphere (effective sphere) are given in Appendix D. The coupling spectra K_n in Eq. (10) can be exploited to extract the modified optomechanical coupling strength of the anisotropic sphere as

$$g_{op,n}^{ani} \approx \sqrt{\frac{\hbar}{2\omega_m}} (\bar{\mathcal{R}} \omega_n^{ani}) \frac{n(n+1)(2n+1)R^{2n+1}}{8\pi\epsilon_0(n\epsilon_{\infty}^{ani} + (n+1))r_m^{2n+4}}. \quad (11)$$

By defining the mode volume of the plasmonic nanocavity (anisotropic sphere) for n^{th} localized surface plasmonic mode as

$$V_n^{ani} = \frac{8\pi(n\epsilon_{\infty}^{ani} + (n+1))r_m^{2n+4}}{n(n+1)(2n+1)R^{2n+1}}, \quad (12)$$

the following expression for the parameter, $g_{op,n}^{ani}$, which introduced in Ref. [12], is recovered:

$$g_{op,n}^{ani} = \bar{\mathcal{R}} \sqrt{\hbar/2\omega_m} (\omega_n^{ani}/\epsilon_0 V_n^{ani}). \quad (13)$$

B. Isotropic spherical nanostructure optomechanically coupled to the SGNR

To demonstrate the role of anisotropy in the dynamics of the system and provide a quantitative comparison with

its isotropic counterpart, we explore results for the second case of an isotropic spherical cavity, i.e., the limiting case $\varepsilon_t = \varepsilon_r$.

In this limit, the modified Mie coefficients that derived in Eqs. (D2a) and (D2b) reduce to the coefficients for the isotropic sphere, as developed in Ref. [47]. Furthermore, the permittivity function in Eq. (8) simplified to the expression with Drude parameters ω_p and ε_∞ for the isotropic sphere. So, we can identify the optomechanical strength and modal volume for isotropic sphere by replacing the Drude-like parameters ω_n^{ani} and ε_∞^{ani} with their limiting parameters ω_n and ε_∞ in Eqs. (11) and (12). In this way, the results in Eqs. (11) and (12) for $AR_\infty = 1$ properly reduce to the corresponding expressions for the isotropic sphere. In section IV, we depict and compare the effects of these physical features on the sensing process for several plasmonic structures.

IV. RESULT AND DISCUSSIONS

A. Optomechanical coupling Strength

In this section, we numerically study the behavior of the optomechanical coupling spectra and strengths for interaction between each plasmonic nanostructure and the SGNR. We compare the obtained results for different plasmonic structures. We then explore the effects of the material, geometrical and modal parameters on the system dynamics and consequently the sensing process.

First of all, we list the physical parameters of the subsystems. Consider a graphene armchair nanoribbon of dimensions $l = 20nm$ and $w \approx 20nm$ with the frequency of the breathing-like mode $\omega_m \approx 470GHz$ [48, 49], and the total mass $m \approx 3 \times 10^{-22}kg$ [50, 51]. The quality factor of the Raman active mode drastically decreases at room temperature. This results in a damping rate of $\gamma = 1.9GHz$. We set the quantum yield of the nanoribbon $\eta = 0.01$ and assume that the square of the Raman tensor element \bar{R} is of order $10^3(A^4a.m.u^{-1})$ [13]. For the isotropic nanocavity, we take into account a silver nanosphere of radius $R = 10nm$ placed at a distance of $r_m = 14nm$ from the graphene nanoribbon, and characterize their dissipative and dispersive properties by the Drude model with typical parameters: $\omega_p = 1.9PHz$, $\Gamma_p = 0.012PHz$, and $\varepsilon_\infty = 6$ [52–54]. For the anisotropic nanocavity in which both radial and tangential components of the permittivity tensor described by the Drude-like model, we also choose the above material parameters for the radial component along with a variable anisotropy ratio. Using these parameters, and Eqs. (9a) and (9b), we can easily get the effective material parameters ε_∞^{ani} and ω_p^{ani} .

We can now analyze the coupling of the SGNR to the plasmonic modes of the nanocavity. The solid curves in Fig. 2 represent the Lorentzian coupling spectra K_n for coupling of the four first LSP_n modes of the silver nanosphere to the SGNR as a function of a dimensionless

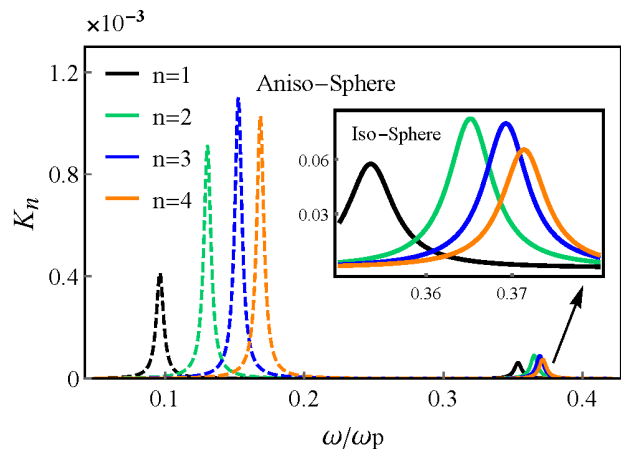


FIG. 2: Optomechanical coupling spectra versus ω/ω_p for coupling of the SGNR to the four first LSP_n modes of the silver sphere (solid curves) and the anisotropic nanosphere (Dashed curves) with $AR_\infty = 0.01$. Here, we set $r_m = 14nm$ and $R = 10nm$. Other material parameters are chosen as $\omega_p = 0.19PHz$, $\omega_m = 470GHz$ and $\gamma = 1.9GHz$. The inset shows the zoomed-in of the spectra for the silver sphere nanocavity.

frequency ω/ω_p . We observe that the Lorentzian peaks associated with the spectral coupling functions K_n start to overlap each other by increasing the order of multipolar coupling n . Thus, it seems the silver sphere nanocavity is not a suitable structure for mass sensing since spectral functions can not be resolved properly and overlap noticeably, especially for higher mode couplings.

Dashed curves in Fig. 2 are related to the Lorentzian peaks for an anisotropic spherical nanocavity manifesting the role of anisotropy in the dynamics of the system. As it is evident, spectral functions are slightly red-shifted and narrowed by decreasing the anisotropy ratio from $AR_\infty = 1$ to 0.01. Furthermore, there is no significant spectral interference compared to the isotropic nanosphere case. Therefore, by manipulating the anisotropy ratio, the Lorentzian curves are split from each other, and the position of peaks can be tuned. All of these features become practically useful in the sensing process and will be addressed in more detail later.

The optomechanical coupling strength corresponding to the interaction between the SGNR and several multipolar modes of the isotropic and anisotropic nanospheres are illustrated as a function of the dimensionless distance $r_m\omega_p/c$ in Figs. 3(a) and 3(b), respectively. One clearly sees that the largest values for the coupling strength belong to the interaction between the plasmonic modes of the anisotropic spherical nanocavity and the SGNR, regardless of the magnitude of n in Fig. 3 (b). Comparing the behavior of the several multipolar couplings in two panels, we find that for separation distances up to $r_m \approx 19nm$, coupling of the SGNR to the higher-order modes plays an essential role in the dynamics of the system. However, the dipolar coupling, $n = 1$, becomes

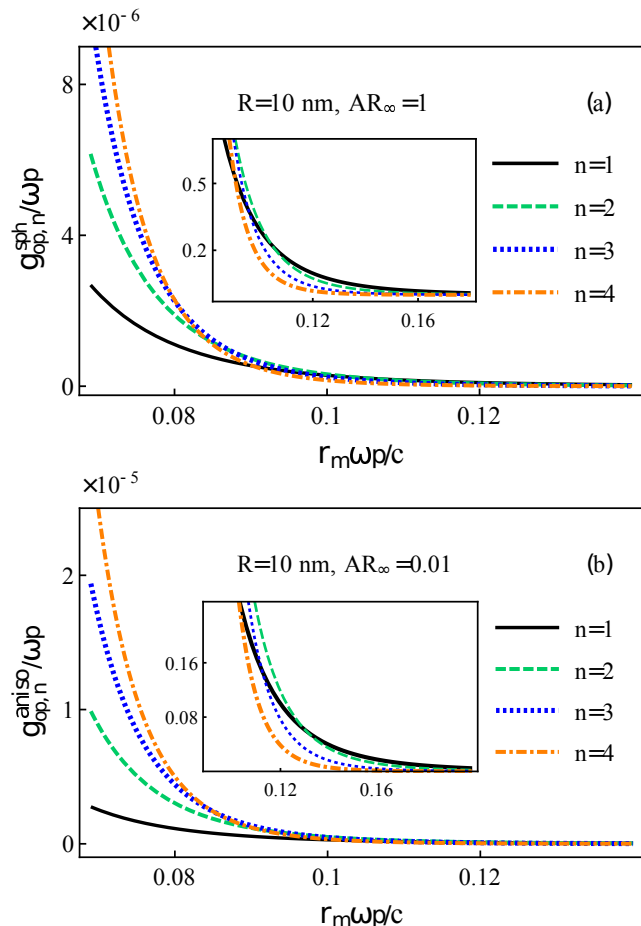


FIG. 3: Optomechanical coupling strength versus $r_m\omega_p/c$ for interaction between the SGNR and four first LSP_n modes of (a) the silver nanosphere, and (b) the anisotropic nanosphere. Values for parameters are the same as those in Fig. 2. The insets show the zoomed-in of the panels within the range $r_m \approx 0.084c/\omega_p$ to $r_m \approx 0.19c/\omega_p$. Scaled separation distances are approximately equivalent to the interval distance $r_m = 11nm - 22nm$.

dominant for large distances. As expected, the optomechanical coupling strength is greater for small separation distances in Figs. 3 (a) and 3 (b).

B. Mass Sensing

Having explained the behavior of the coupling strength, we now present numerical results for mass sensing through the pump-probe technique [55–57]. Our purpose is to manipulate the geometrical and material features of the spherical nanostructures to see how the probe spectrum is effected at room temperature. Using Eqs. (C4) and (C5), we can obtain the transmission spectrum of the probe field. In Fig. 4(a), we have illustrated the probe fields transmission spectra for the optomechanical

couplings of the isotropic and anisotropic nanospheres to the SGNR in terms of the probe-cavity detuning δ at fixed separation distance $r_m = 14nm$. Notice that here δ is specifically defined as $\delta = \omega_1 - \omega_{pr}$, which corresponds to the dipolar coupling.

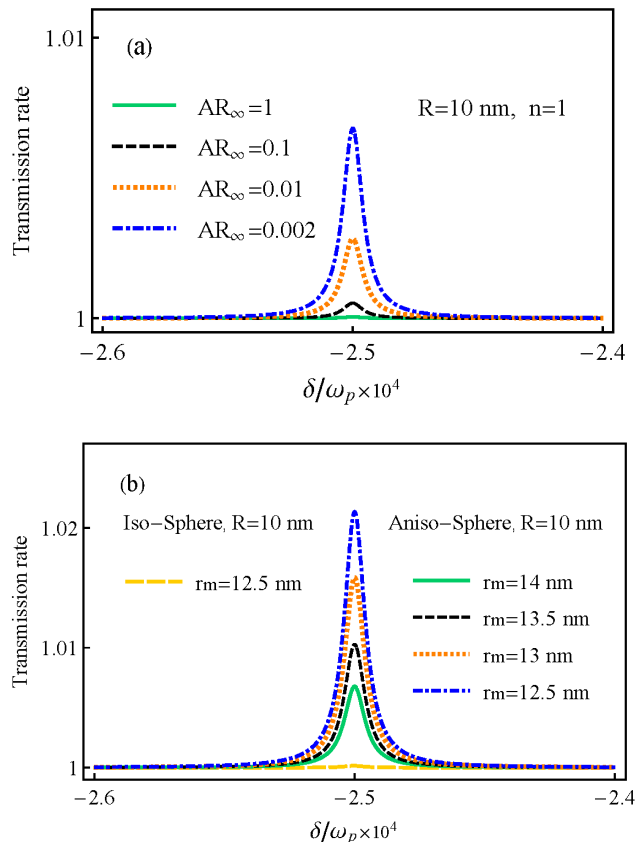


FIG. 4: Transmission rate versus δ/ω_p for dipolar coupling of the SGNR to (a) the silver nanocavity, and (b) the anisotropic nanosphere with $AR_\infty = 0.002$. Values for other parameters are the same as those in Fig. 2.

We analyze the results for $AR_\infty = 0.1$ (black dashed curve), $AR_\infty = 0.01$ (orange dotted curve) and $AR_\infty = 0.002$ (blue dot-dashed curve). It is seen that the strength of the transmission peak enhances by decreasing AR_∞ from 1 for the isotropic silver nanosphere (green curve) to the smaller value for the anisotropic nanosphere. It is related to the role of mode volume as well as damping rate of plasmonic nanocavities. Traditional CQED investigates the dynamics of atom-field interaction by exploring the influences of the cavity quality factor, while in the PCQED the key parameter is mode volume [9, 41]. Plasmonic nanocavities confine electromagnetic energy beyond the classical diffraction limit, resulting in small mode volumes. Since coupling strength is inversely proportional to the mode volume, the nanostructures with smaller mode volume provide larger coupling strength and consequently higher transmission peak. When the

anisotropy ratio decreases from the value $AR_\infty = 1$ to $AR_\infty = 0.01$, the enhancement of the optomechanical coupling strength occurs due to mode volume reduction. This is verified by the plots in Figs. 3(a) and 3(b), in which the optomechanical coupling strength of the SGNR to the anisotropic nanocavity modes with $AR_\infty = 0.01$ is stronger than the silver sphere modes regardless of the order of interaction.

It is worth noting that further reduction of the anisotropy ratio leads to the smaller optomechanical coupling strengths compared to the value of 0.01 (here the figure is not presented for the sake of brevity). But on the other hand, the redshift of the resonance frequencies leads to the enhancement of the coupling functions between the plasmonic field and the classical incident fields (Ω_{pu}, Ω_{pr}). These features provide a higher transmission peak for the smaller anisotropy ratio, as shown in Fig. 4(a).

For nanostructures with a small radius, plasmonic damping rate comprises two terms: the Joule term that accounts for electron scattering losses, and the radiative damping term [44, 45]. Having estimated the damping rates related to the dipolar mode of the two plasmonic nanocavities, we find that the total damping rate of the anisotropic nanosphere becomes slightly smaller than the damping rate of the silver sphere nanocavity due to the smaller contribution of the radiative damping term.

In Fig. 4(b), we illustrate the influence of separation distance r_m on the probe transmission spectrum for dipolar coupling of the anisotropic nanosphere to the SGNR. Here, the results are depicted for a fixed anisotropy ratio $AR_\infty = 0.002$. As expected, when the SGNR gets closer to the surface of the anisotropic nanosphere, the intensity of the transmission peak enhances slightly which makes it easier to detect for sensing purposes. For the SGNR placed $4nm$ away from the anisotropic nanosphere surface, the result is shown with the green-solid curve in Fig. 4(b). We observe that the peak intensity for the anisotropic nanosphere at a farther distance is greater than that for the isotropic sphere at a shorter distance (yellow-solid line). Notice that for distances less than $r_m = 11nm$, nonlocal effects become increasingly pronounced, which are out of the scope of the present study.

So far, we have examined the effects of the anisotropy ratio and separation distance on the transmission spectrum. In Fig. 5(a), we compare the behavior of the spectrum peaks for the coupling of the SGNR to the three first LSP_n modes of the anisotropic nanosphere. Here, we set $AR_\infty = 0.002$ and $r_m = 12.5nm$. Results indicate that close to the surface of spherical nanocavity, higher-order mode coupling exhibits a higher peak intensity.

The sensing process with a weak incident pump field provides a suitable platform for the exploration of living organisms' features. Therefore, in Fig. 5(b), we have depicted the transmission peak strength for the probe field in terms of the incident pump intensity of the order $I_{pu} \approx 10KW/cm^2$. The corresponding results for higher intensities are plotted in the inset of Fig. 5(b).

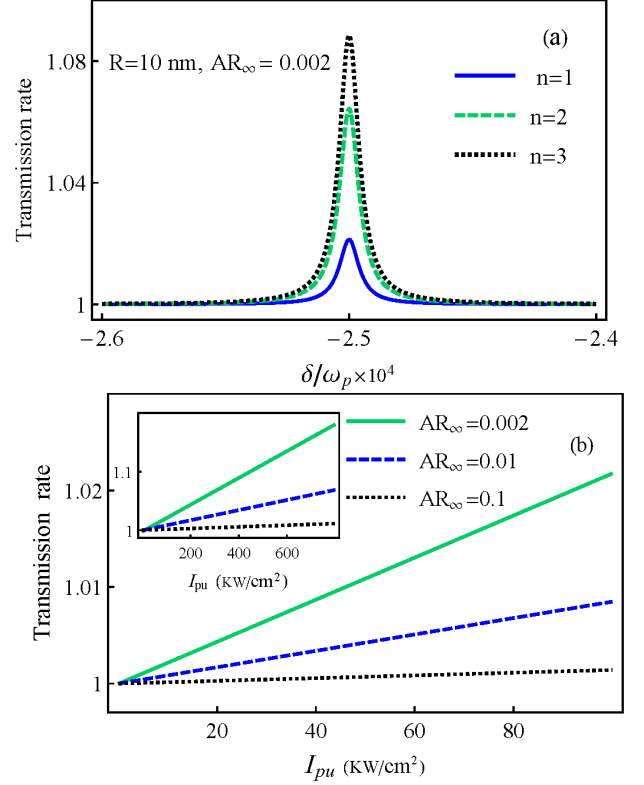


FIG. 5: (a) Transmission rate versus δ/ω_p for coupling the SGNR to several multipolar modes of the anisotropic sphere with $R = 10nm$ and $r_m = 12.5nm$. (b) Transmission rate versus incident pump intensity. Other parameter values are $\omega_p = 0.19PHz$, $\omega_m = 470GHz$ and $\gamma = 1.9GHz$.

The extremely small size of the SGNR makes physical properties greatly sensitive to the perturbations originating from the external force and mass adsorbed on it. Based on the relationship between mass changes of the graphene nanoribbon and its frequency shift, one can perform a sensing process through the relation $\Delta m = (2m)\Delta\omega/\omega_m$ [48]. In the pump-probe scheme, the frequency shift induced by the molecular species loaded onto the nanoribbon surface is monitored. Minimal measurable mass depends on the bandwidth of the absorption spectrum. To understand the accuracy of mass sensing in this system, we make a numerical estimation in the following.

As it is evident from the black dot curve in Fig. 5(a), the octupolar coupling results in the highest peak for the transmission spectrum at the separation distance $r_m = 12.5nm$ when the anisotropic nanosphere is illuminated with the incident pump intensity $I_{pu} \approx 400KW/cm^2$. Therefore, we can estimate FWHM (full width at half maximum) of the probe spectrum for the black dot curve in Fig. 5(a), which is $\Delta\omega \approx 0.18GHz$. The calculation indicates that the minimum resolution for mass sensing

takes the value $\Delta m \approx 1.2 \times 10^{-24} kg$. For lower intensities of order, $I_{pu} \approx 40 KW/cm^2$, the height of the transmission peak reduces to the approximate value 0.01. However, the accuracy of mass sensing becomes almost the same as before.

Notice that the analytical method introduced here can be generalized to include a variety of plasmonic nanocavities as the optical subsystem. For multilayered plasmonic nanostructures, optical properties can be adjusted more accurately due to the tunable geometrical and material parameters of these structures. This feature makes plasmonic nanocavities attractive for sensing applications since the optomechanical coupling strength, as well as the plasmonic damping rate, can be adjusted more effectively through manipulating optical features of these multilayered nanostructures. Tunable plasmonic damping rate and coupling strength affect the width and height of the probe transmission spectrum, respectively. Thus, an anisotropic spherical nanoshell (core) in combination with the metallic core (nanoshell), which can provide mass sensing with higher precision, will be the subject of our next study.

In the end, the nanomechanical subsystem may be affected by the thermomechanical and momentum exchange noises, as well as the Casimir force. The contribution of the first two effects is negligible at room temperature (see Ref. [58]), while an approximate estimation of the Casimir force to examine its effect on the sensing process is needed. Bimonte et al. derived a semi-analytic formula, $F_c = -(\pi^3 \hbar c R / 360 h^3)$, for the sphere-plate Casimir force, in which R is the radius of the spherical structure, and h represents the separation distance between the plate and surface of metallic sphere [59]. For parameter values $R = 10 nm$ and $h = 3 nm$, the Casimir force takes the value $F_c = 9 \times 10^{-27} N$. In another study, Biehs et al. investigated the Casimir-Polder force between a gold nanoparticle and a single sheet of pristine graphene in detail [60]. They have shown that although the graphene sheet behaves like a perfect metal for distances larger than the thermal wavelength, for small distances the Casimir-Polder force is relatively small compared to the values of the ideal metal case and depends on the Fermi level of the graphene sheet. Bearing this in mind, it is clear that the weight of the minimum measurable mass would be still comparable with the Casimir force.

V. SUMMARY AND CONCLUSION

In this paper, we have investigated the anisotropy effects of nanocavity on mass sensing in the molecular plasmonic system. To do so, we have presented a formalism that allows us to manipulate the transmission spectrum of the probe field for mass sensing through the pump-probe technique. In this manner, the molecular plasmonic system is mapped onto the cavity optomechanical model [13, 14], then the mode-selective quantization

scheme presented in Ref. [26] is extended to formulate a multimode Hamiltonian of the optomechanical system.

It is shown that the geometrical, material, and modal considerations, which are relevant to the plasmonic subsystem, are contained in the Hamiltonian through the electromagnetic Green's tensor. We found the explicit form of the optomechanical coupling strength, the parametric interaction between the plasmonic mode, and the Raman active mode of the SGNR in terms of the symmetrical and geometrical properties of the graphene nanoribbon and plasmonic nanocavity. Taking symmetry properties of the nanoribbon into account, we determined the coupling spectral function and optomechanical strength for some spherical plasmonic structures by extracting their Green tensors. We showed that an anisotropic nanocavity with a small anisotropy ratio is more suitable for the sensing process. Furthermore, the manipulation of anisotropy features of the plasmonic nanocavity made it possible to reduce mode volume (enhance optomechanical strength) and damping rate for optimal mass sensing. We then have illustrated transmission spectra for two cases of plasmonic nanostructures. The results indicated an enhancement in the transmission peak corresponding to the anisotropic nanocavity, and verified its superiority over the isotropic one for sensing applications.

In a traditional optomechanical system, a high-Q microcavity at cryogenic temperature is needed to accurately perform mass sensing. Recently, mass sensing with the precision of order $10^{-26} kg$ is performed in molecular plasmonic systems with low-Q plasmonic nanocavities (cylindrical dimer) at room temperature [22]. Of course, we can attribute this high efficiency to the small mode volume of the plasmonic nanocavity, and as well a controversial frequency considered for the breathing-like mode of the graphene nanoribbon. Unlike the previous work developed by Liu, as a main purpose of this paper, we have presented an analytical method to explicitly calculate the mode volume and damping rate of plasmonic modes for different plasmonic nanocavities. Of course, improving the accuracy of the current mass sensing device and achieving the highest accuracy by engineering the plasmonic multilayered nanostructures is under consideration.

Appendix A: Mode-selective quantization approach

The Green's tensor contains all modal information of the plasmonic structure. Following the method developed in Refs. [26, 27], we consider a spherical geometry for which the Green's tensor can be decomposed as a sum over the discrete modes (multipole expansion with spherical symmetry):

$$\bar{\mathbf{G}}(\mathbf{r}_m, \mathbf{r}, \omega) = \sum_{n=1}^{\infty} \bar{\mathbf{G}}_n(\mathbf{r}_m, \mathbf{r}, \omega), \quad (\text{A1})$$

where index n represents the radial harmonic index and $\bar{\mathbf{G}}_n(\mathbf{r}_m, \mathbf{r}, \omega)$ contains contribution of the LSP_n (dipolar

plasmon for $n = 1$, quadrupole plasmon for $n = 2$, etc.). Similar to the Green tensor, the electric field operator associated with the plasmonic structure can be written in terms of the several multipole components

$$\hat{\mathbf{E}}(\mathbf{r}_m, \omega) = \sum_{n=1}^{\infty} \hat{\mathbf{E}}_n(\mathbf{r}_m, \omega). \quad (\text{A2})$$

The component $\hat{\mathbf{E}}_n(\mathbf{r}_m, \omega)$ describes the electric field operator associated with the LSP_n . Point group theory tells us that the fundamental vibration of nanoribbon with the breathing-like displacement of the phonon mode has the A_g symmetry (diagonal Raman tensor) just for special scattering patterns of a doubly clamped nanoribbon [30, 35]. If this condition is met, the spectral decomposition of the electric field operator in the frequency domain leads to the simplified form of the interaction Hamiltonian in Eq. (2) as

$$\hat{H}_{int} = -\sqrt{\frac{\hbar}{2\omega_m}}(\hat{b} + \hat{b}^\dagger) \int \int d\omega d\omega' \mathcal{R}_{ii} \quad (\text{A3})$$

$$\times \left\{ \hat{E}_i^{(-)}(\mathbf{r}_m, \omega) \hat{E}_i^{(+)}(\mathbf{r}_m, \omega') + \hat{E}_i^{(+)}(\mathbf{r}_m, \omega) \hat{E}_i^{(-)}(\mathbf{r}_m, \omega') \right\},$$

where \mathcal{R}_{ii} are diagonal elements of the SGNR Raman tensor with $i = x, y, z$ (here the Einstein's sun convention is used). In the above Hamiltonian, we have neglected two terms in Eq. (A3) since they don't satisfy the energy conservation. Up to now, we have considered the localized plasmon polaritons in a continuous band description. However, the dynamic of the composite system is based on the excitation of the LSP modes of the spherical nanostructure by an external pump laser and optomechanical coupling to the vibrational mode of the mechanical subsystem. Therefore, based on the scheme of the mode-selective quantization developed in Refs. [26, 27], along with Gram-Schmidt orthogonalization procedure, we suppose that N discrete modes participate in the coupling process. In this manner, we introduce mode-selective bosonic annihilation operator as

$$\hat{a}_n(\mathbf{r}_m, \omega) = \sqrt{\mathcal{R}_{ii}/(2\omega_m \hbar)}^{1/2} \alpha_n(\omega) \hat{e}_i \hat{E}_{n,i}^{(+)}(\mathbf{r}_m, \omega), \quad (\text{A4})$$

where $\hat{e}_i (i = 1, 2, 3)$ are the cartesian unit vectors. The operator $\hat{a}_n(\mathbf{r}_m, \omega)$ is associated with the LSP_n mode at the position of the nanoribbon and can be excited by the external laser at a given position of the mechanical resonator. It is worth noting that the introduced mode-selective bosonic operators satisfy the usual bosonic commutation relation $[\hat{a}_n(\mathbf{r}_m, \omega), \hat{a}_m^\dagger(\mathbf{r}_m, \omega')] = \delta(\omega - \omega') \delta_{nm}$, provided that $\alpha_n(\omega)$ is given by relation $|\alpha_n(\omega)|^2 = 1/|k_n(r, \omega)|^2$ with

$$|k_n(\mathbf{r}, \omega)|^2 = (\mathcal{R}_{ii} k_1^2 / \pi \epsilon_0) \quad (\text{A5})$$

$$\times \sqrt{\hbar/2\omega_m} \hat{e}_i \cdot [\text{Im} \bar{\mathbf{G}}_{n,s}(\mathbf{r}_m, \mathbf{r}, \omega)] \cdot \hat{e}_i.$$

Employing the quantization method, the interaction part of the Hamiltonian can be obtained in terms of frequency

dependent bosonic operator $\hat{a}_n(\mathbf{r}_m, \omega)$ and the spectral coupling functions $k_{n,m}(\mathbf{r}_m, \omega)$. To completely perform the mode-selective quantization scheme and obtain the final effective Hamiltonian, we need to determine the explicit form of the spectral function. Considerations related to the symmetrical and vibrational properties of the phonon modes, as well the electromagnetic Green's tensor help us to identify the form of $k_n(\mathbf{r}_m, \omega)$. For an armchair graphene ribbon in the xy plane with the periodicity direction along y , the A_g mode is Raman active for geometry $(zXxz)$. Here $zz(XX)$ represent the propagation (polarizations) directions of the incident and scattered light, respectively [30, 35, 36]. Based on the properties of the A_g symmetrized Raman tensor, we only need diagonal components of the scattering Green's tensor $\bar{\mathbf{G}}_{s,ii}^{(11)}(\mathbf{r}_m, \mathbf{r}_m)$ with $i = x$. By applying symmetry arguments, the optomechanical coupling spectra, $K_n = |k_n(r_m, \omega)|^2$, is obtained as following

$$K_n = (\mathcal{R}_{ii} k_1^2 / \pi \epsilon_1) \sqrt{\hbar/2\omega_m} \text{Im} \left[\bar{\mathbf{G}}_{n,s}(\mathbf{r}_m, \mathbf{r}_m, \omega) \right]_{ii}. \quad (\text{A6})$$

Finding the general form of spectral function, we can go one step further and introduce new frequency-independent plasmonic operators $\hat{a}_n(r_m)$ at the position of the nanoribbon

$$\hat{a}_n(\mathbf{r}_m) = \beta_n \int d\omega k_n(\mathbf{r}_m, \omega) \hat{a}(\mathbf{r}_m, \omega). \quad (\text{A7})$$

The coefficient β_n is determined through the relation $|\beta_n|^2 = 1/\int d\omega |k_n(r_m, \omega)|^2$ so that these new-defined plasmonic operators satisfy the bosonic commutation relation as $[\hat{a}_n(\mathbf{r}_m), \hat{a}_m^\dagger(\mathbf{r}_m)] = \delta_{nm}$. The effective Hamiltonian is obtained by integrating over the angular frequency to establish a set of N discrete modes.

Appendix B: Derivation of the free field Hamiltonian for plasmonic subsystem

In the following, we indicate the main steps toward deriving the quantum Langevin equation and free field Hamiltonian of the plasmonic subsystem. Based on the methods developed in Refs. [26, 27], we can decompose the plasmonic part of the free field Hamiltonian into the predefined bright mode and a set of continuous non-interacting orthogonal dark modes

$$\hat{d}(\mathbf{r}, \omega) = \hat{f}(\mathbf{r}, \omega) - \sum_{n=1}^N \left[\hat{f}(\mathbf{r}, \omega), \hat{a}_n^\dagger(\mathbf{r}_m, \omega) \right] \hat{a}_n(\mathbf{r}_m, \omega). \quad (\text{B1})$$

Since dark modes have independent dynamics and will not affect the dynamics of the bright modes, after some algebraic calculations, we arrive at the relation

$$\int d^3r \hat{f}^\dagger(\mathbf{r}, \omega) \hat{f}(\mathbf{r}, \omega) = \sum_{n=1}^N \hat{a}_n^\dagger(\mathbf{r}_m, \omega) \hat{a}_n(\mathbf{r}_m, \omega) \quad (\text{B2})$$

$$+ \int d^3r \hat{d}^\dagger(\mathbf{r}, \omega) \hat{d}(\mathbf{r}, \omega).$$

The term related to the free Hamiltonian of dark modes can be omitted since it plays no role in the dynamic of the system. To determine the plasmonic part of the Hamiltonian based on the frequency-independent bosonic operator, we first start with the quantum Langevin equation for the new plasmonic operator, $d\hat{a}_{n'}(\mathbf{r}_m)/dt = [\hat{a}_{n'}(\mathbf{r}_m), \hat{H}_0]/i\hbar$, in which the Hamiltonian \hat{H}_0 is defined as

$$\hat{H}_0 = \int d\omega \hbar \omega \sum_{n=1}^N \hat{a}_n^\dagger(\mathbf{r}_m, \omega) \hat{a}_n(\mathbf{r}_m, \omega). \quad (\text{B3})$$

Here, we have used the definition of bosonic annihilation operator $\hat{a}_n(\mathbf{r}_m, \omega)$ in the position of the SGNR to rewrite the Langevin equation as

$$\dot{\hat{a}}_{n'}(\mathbf{r}_m) = - \int d\omega \omega k_{n'}(\mathbf{r}_m, \omega) \hat{a}_{n'}(\mathbf{r}_m, \omega) / g_{n'}(\mathbf{r}_m). \quad (\text{B4})$$

Eq. (B4) is not yet a closed equation for $\hat{a}_{n'}(\mathbf{r}_m)$, since there is an additional integral kernel apart from the definition of the operators $\hat{a}_{n'}(\mathbf{r}_m)$. To get a closed-form, we subtract and add the term $(-\omega_n + i\Gamma_n/2)$ to the integral kernel, and then use the relation

$$k_n(\mathbf{r}_m, \omega) = \sqrt{(\Gamma_n/2\pi)} (ig_n(\mathbf{r}_m) / (\omega - \omega_n) + i\Gamma_n/2). \quad (\text{B5})$$

We arrive at the following quantum Langevin equation that includes the quantum noise and dissipation terms

$$\dot{\hat{a}}_{n'}(\mathbf{r}_m) = -i\omega_n \hat{a}_{n'}(\mathbf{r}_m) - (\Gamma_n/2) \hat{a}_{n'}(\mathbf{r}_m) + \hat{F}_{n'}(\mathbf{r}_m). \quad (\text{B6})$$

Here, the quantum noise is defined as $\hat{F}_{n'}(\mathbf{r}_m) = -i \int d\omega \sqrt{(\Gamma_n/2\pi)} \hat{a}_{n'}(\mathbf{r}_m, \omega)$. Eq. (B6) now can be considered as the quantum Langevin equation for the new plasmonic operator with respect to the Hamiltonian $\hat{H}_p = \sum_{n=1}^N \hbar \omega_n \hat{a}_n^\dagger(\mathbf{r}_m) \hat{a}_n(\mathbf{r}_m)$. In the end, incorporating the nanoribbon Hamiltonian and as well its interaction term in the equation of motion, we get

$$\dot{\hat{a}}_{n'}(\mathbf{r}_m) = [\hat{a}_{n'}(\mathbf{r}_m), \hat{H}_{sys}] / i\hbar - (\Gamma_n/2) \hat{a}_{n'}(\mathbf{r}_m) + \hat{F}_{n'}(\mathbf{r}_m). \quad (\text{B7})$$

Appendix C: Linearization of the Quantum Langevin equations in pump-probe technique

Heisenberg equations of motion for the plasmonic annihilation operator and the mean response of the mechanical subsystem, $\hat{n} = \hat{b} + \hat{b}^\dagger$, are given by

$$\dot{\hat{a}}_n(\mathbf{r}_m) = -(i\Delta_n + \kappa_n) \hat{a}_n(\mathbf{r}_m) + ig_{op,n} \hat{a}_n(\mathbf{r}_m) \hat{n} + \Omega_{pu} + \Omega_{pr} \exp(-i\delta t) + \hat{F}_n(\mathbf{r}_m), \quad (\text{C1a})$$

$$\ddot{\hat{n}} + \gamma \dot{\hat{n}} = -\omega_m^2 \hat{n} + 2\omega_m g_{op,n} \hat{a}_n^\dagger(\mathbf{r}_m) \hat{a}_n(\mathbf{r}_m) + \hat{\xi}(t). \quad (\text{C1b})$$

Eq. (C1a) represents the dynamics of the n^{th} plasmonic mode. The correlations associated with the quantum vacuum fluctuations of the plasmonic cavity modes are fully characterized by the δ -correlation functions as developed in Refs. [15, 41]. In Eq. (C1b), γ and $\hat{\xi}(t)$ represent the damping rate and Brownian noise of the SGNR, respectively. Here, the SGNR is affected by a Brownian stochastic force with zero mean value and the correlation function that is given in Ref. [15]. Since the incident probe field is much weaker than the pump field, we employ the perturbation method to investigate the optical properties of the system [22]. In the pump-probe technique, the Heisenberg operators can be decomposed as the sum of a steady-state mean value and a small fluctuation with zero mean value, i.e., $\hat{a}_n(t) = \bar{a}_n + \delta\hat{a}_n(t)$ and $\hat{n}(t) = \bar{n} + \delta\hat{n}(t)$ with the steady-state mean values $\bar{a}_n = \hat{a}_{n0}$ and $\bar{n} = n_0$. To obtain the steady-state solutions of the operators, we set the time derivatives of operators in the Eqs. (C1a) and (C1b) equal to zero, and yields: $a_{n0} = \Omega_{pu} / (i(\Delta_n - g_{op,n}n_0) + \kappa_n)$, and $n_0 = 2g_{op,n} \omega_0 / \omega_m$ with $\omega_0 = |a_{n0}|^2$.

Inserting these definitions in Eqs. (C1a) and (C1b), and neglecting the terms $\delta\hat{a}_n(t)\delta\hat{n}(t)$, quantum Langevin equations govern the time evolution of the fluctuation operators can be derived as

$$\delta\dot{\hat{a}}_n(\mathbf{r}_m) = -(i\Delta_n + \kappa_n) \delta\hat{a}_n(\mathbf{r}_m) + ic_0 g_{op,n} \delta\hat{n} + in_0 g_{op,n} \delta\hat{a}_n(\mathbf{r}_m) + \Omega_{pr} e^{-i\delta t} + \hat{F}_n(\mathbf{r}_m), \quad (\text{C2a})$$

$$\delta\ddot{\hat{n}} = -\gamma \delta\dot{\hat{n}} - \omega_m^2 \delta\hat{n} + 2c_0 \omega_m g_{op,n} \delta\hat{a}_n^\dagger(\mathbf{r}_m) + 2c_0^* \omega_m g_{op,n} \delta\hat{a}_n(\mathbf{r}_m) + \xi(t). \quad (\text{C2b})$$

We identify all fluctuation operators with their expectation values and eliminate the noise terms. To solve these set of equations, we use the following ansatz in the rotating frame

$$\langle \delta\hat{a}_n(\mathbf{r}_m) \rangle = a_{n+} \exp[-i\delta t] + a_{n-} \exp[i\delta t], \quad (\text{C3a})$$

$$\langle \delta\hat{n} \rangle = n_+ \exp[-i\delta t] + n_- \exp[i\delta t]. \quad (\text{C3b})$$

Now we substitute these equations into Eqs. (C2a) and (C2b), then equate the terms with the same time dependence, and finally find the solution for a_{n+} as below

$$a_{n+} = \frac{\Omega_{pr} [w(x_n - y_n) + z_n]}{w(x_n^2 - y_n^2) + 2y_n z_n}. \quad (\text{C4})$$

Eq. (C4) is given in the lowest order in Ω_{pu} but to all orders of Ω_{pr} . Here, the parameter w , and functions z_n , y_n and x_n are defined as $w = -(\delta^2 + i\gamma\delta + \omega_m^2)$, $z_n = 2i(\omega_m \omega_0) g_{op,n}^2$, $y_n = i\Delta_n - in_0 g_{op,n}$ and $x_n = \kappa_n - i\delta$. To investigate the optical response of the system via the output field, we employ the input-output relation $\hat{a}_{n,out}(t) + \hat{a}_{n,in}(t) = \sqrt{2\kappa_n} \hat{a}_n(t)$ [15]. Given that the mean value of the input operator $\hat{a}_{n,in}(t)$ is equal to zero, we obtain

$$\begin{aligned} \langle \hat{a}_{n,out}(t) \rangle &= a_{n0,out} + a_{n+,out} e^{-i\delta t} + a_{n-,out} e^{i\delta t} \\ &= \sqrt{2\kappa_n} (a_{n0} + a_{n+} e^{-i\delta t} + a_{n-} e^{i\delta t}). \end{aligned} \quad (\text{C5})$$

Appendix D: Mie coefficients of the Green's tensor for an anisotropic sphere

The electromagnetic Green's tensor for a radial anisotropic sphere has been extracted previously in Ref. [42]. When the field and the source points locate in the first layer, the electromagnetic Green tensor can be separated into two parts of the vacuum and the scattering. The former describes the contribution of the direct waves from the source in the free space. The latter represents the contribution of the multiple transmission and reflection waves that occur due to interfaces. The role of anisotropy of the plasmonic structure is in-

cluded in the Green tensor through a non-integer order $v = [n(n+1)AR + 1/4]^{1/2} - 1/2$ and an anisotropy ratio $AR = \varepsilon_t/\varepsilon_r$. By imposing the boundary conditions and employing the recursive algorithm method, all the unknown scattering Mie coefficients can be determined. For the spherical structure under study, the Mie coefficients can be obtained in terms of the transmission T-matrix elements as follows

$$B_l^{(11)} = -T_{l,12}^{(1)}/T_{l,11}^{(1)}, \quad (D1)$$

with $l = N, M$. For $l = N$, the elements of the transformation matrix is given by [42]

$$T_{N,11}^{(1)} = \frac{\psi_v(k_t R)\zeta'_n(k_1 R)/\eta_t - \zeta_n(k_1 R)\psi'_v(k_t R)/\eta_1}{\psi_v(k_t R)\zeta'_v(k_t R)/\eta_t - \zeta_v(k_t R)\psi'_v(k_t R)/\eta_t}, \quad (D2a)$$

$$T_{N,12}^{(1)} = \frac{\psi_v(k_t R)\psi'_n(k_1 R)/\eta_t - \psi_n(k_1 R)\psi'_v(k_t R)/\eta_1}{\psi_v(k_t R)\zeta'_v(k_t R)/\eta_t - \zeta_v(k_t R)\psi'_v(k_t R)/\eta_t}, \quad (D2b)$$

where $k_t^2 = \omega^2 \varepsilon_t \mu_t / c^2$, $\eta_t = \sqrt{\mu_t / \varepsilon_t}$, and $\psi_v(z)$ ($\zeta_v(z)$) represents the spherical Riccati-Bessel (Riccati-Hankel) function:

$$\psi_v(z) = z j_\nu(z), \quad (D3a)$$

$$\zeta_v(z) = z h_\nu^{(1)}(z). \quad (D3b)$$

These functions and their derivatives in the QSA are defined as

$$\psi_v(z) \sim \frac{z^{v+1}}{2^{v+1}\Gamma(v+3/2)}, \quad (D4a)$$

$$\zeta_v(z) \sim \frac{(-i)2^v(-1)^{v+1}\sqrt{\pi}}{z^v\Gamma(-v+1/2)}, \quad (D4b)$$

$$\psi'_v(z) \sim \frac{\sqrt{\pi}(v+1)z^v}{2^{v+1}\Gamma(v+3/2)}, \quad (D4c)$$

$$\zeta'_v(z) \sim \frac{(-i)2^v(-1)^{v+1}\sqrt{\pi}(-v)}{z^v\Gamma(-v+1/2)}. \quad (D4d)$$

Now, by substituting Eqs. (D4a)-(D4d) into Eqs. (D2a) and (D2b), the Mie coefficient $B_N^{(11)}$ is given by

$$B_N^{(11)} = \frac{i(k_1 R)^{2n+1}[(n+1)\varepsilon_t - (v+1)]}{(2n-1)!!(2n+1)!![n\varepsilon_t + (v+1)]}. \quad (D5)$$

In the first layer, i.e., the free space, the non-integer order v reduces to the integer value n . Moreover, the imaginary part of the Mie coefficient $B_M^{(11)}$ vanishes, so it has no contribution to the optomechanical coupling spectra in

the QSA. By defining the effective permittivity as

$$\varepsilon_{eff}^{ani} = \varepsilon_r \left[[n(n+1)\varepsilon_t/\varepsilon_r n^2 + 1/4n^2]^{1/2} - 1/2n \right], \quad (D6)$$

the polarizability of the anisotropic sphere takes exactly the same form as the polarizability of an effective sphere

$$\alpha^{ani} = \frac{n(\varepsilon_{eff}^{ani} - 1)R^{2n+1}}{n\varepsilon_{eff}^{ani} + (n+1)}, \quad (D7)$$

with effective Drude-like parameters that are introduced in section III. Now we can identify the imaginary part of the tangential Green's tensor and the spectral function.

The resonance frequency ω_n^{ani} , which corresponds to the $LSPn$ mode of the effective sphere in Eq. (10), can be expressed as

$$\omega_n^{ani} = \omega_{p,eff}^{ani} \sqrt{n/[n\varepsilon_{\infty,eff}^{ani} + (n+1)]}, \quad (D8)$$

and the total width is $\Gamma_n^{ani} = \Gamma_p^{ani} + \Gamma_{nrad}^{ani}$. First term in Γ_n^{ani} indicates the ohmic loss and the second term represents radiation damping rate Γ_{nrad}^{ani} which is given by

$$\Gamma_{nrad}^{ani} = \frac{\omega_n^{ani}(2n+1)(n+1)(k_n R)^{2n+1}}{n[n\varepsilon_{\infty,eff}^{ani} + (n+1)](2n-1)!!(2n+1)!!}. \quad (D9)$$

This term is added to the ohmic loss to take into account the variation of the electric field over the particle size [44, 45]. It is obvious that for $\varepsilon_t = \varepsilon_r$, the spherical Bessel and Hankel functions of the order ν and Drude-like parameters reduce to, respectively, the spherical Bessel and Hankel functions of the order n and the corresponding Drude parameters for the isotropic sphere. In this limit, the obtained Mie coefficients would be the same as those for the isotropic sphere [47].

-
- [1] M. S. Tame, K. R. McEnery, S. K. zdemir, J. Lee, S. A. Maier, and M. S. Kim, "Quantum plasmonics," *Nat. Phys.* **9**, 329 (2013).
- [2] T. Neuman, R. Esteban, D. Casanova, F. J. Garca-Vidal and J. Aizpurua, "Coupling of molecular emitters and plasmonic cavities beyond the point-dipole approximation," *Nano Lett.* **6**, 2358 (2018).
- [3] J. T. Hugall A. Singh, and N. F. van Hulst, "Plasmonic cavity coupling," *ACS Photonics.* **5**, 43 (2018).
- [4] M.I. Stockman, K. Kneipp, S. I. Bozhevolnyi, S. Saha, A. Dutta, J. Ndukaife, N. Kinsey, H. Reddy, U. Guler, V.M. Shalaev and A. Boltasseva, "Roadmap on plasmonics," *J. Opt.* **20**, 043001 (2018).
- [5] R. Chikkaraddy, B. De Nijs, F. Benz, S. J. Barrow, O. A. Scherman, E. Rosta, A. Demetriadou, P. Fox, O. Hess, and J. J. Baumberg, "Single-molecule strong coupling at room temperature in plasmonic nanocavities," *Nature.* **535**, 127 (2016).
- [6] X. Xiong, L. Wu, X. F. Ren, C. E. Png, G. C. Guo, and Y. F. Xiao, "Quantum plasmonics: new opportunity in fundamental and applied photonics," *Adv. Opt. Photonics.* **10**, 703 (2018).
- [7] J. Zhang, L. Zhang, L. and W. Xu, "Surface plasmon polaritons: physics and applications," *J. Appl. Phys.* **45**, 113001 (2012).
- [8] A. Balytis, Y. Nishijima, S. Krishnamoorthy, A. Kuchmizhak, P. R. Stoddart, R. Petrukevicius, and S. Juodkazis, "From fundamental toward applied SERS: shared principles and divergent approaches," *Adv. Opt. Mater.* **6**, 1800292 (2018).
- [9] P. Ginzburg, "Cavity quantum electrodynamics in application to plasmonics and metamaterials," *Rev. Phys.* **1**, 120 (2016).
- [10] S. Y. Ding, E. M. You, Z. Q. Tian, and M. Moskovits, "Electromagnetic theories of surface-enhanced Raman spectroscopy," *Chem. Soc. Rev.* **46**, 4042(2017).
- [11] M. Fleischmann, P.J. Hendra A. J. McQuillan, "Raman spectra of pyridine adsorbed at a silver electrode," *Chem. Phys. Lett.* **26**, 163 (1974).
- [12] Y. D. Yin, L. Goa, C. W. Qiu, "Electromagnetic theory of tunable SERS manipulated with spherical anisotropy in coated nanoparticles," *Phys. Chem C* **115**, 8893 (2011).
- [13] P. Roelli, C. Galland, N. Piro, and T. J. Kippenberg, "Molecular cavity optomechanics as a theory of plasmon-enhanced Raman scattering," *Nat. Nanotechnol.* **11**, 164(2016).
- [14] M. K. Schmidt, R. Esteban, F. Benz, J. J. Baumberg, and J. Aizpurua, "Linking classical and molecular optomechanics descriptions of SERS," *Faraday Discuss.* **205**, 31 (2017).
- [15] M. Aspelmeyer, T. J. Kippenberg and F. Marquardt, "Cavity optomechanics," *Rev. Mod. Phys.* **86**, 1391 (2014).
- [16] M. k. Schmidt and J. Aizpurua "Nanocavities: optomechanics goes molecular," *Nat. Nanotechnol.* **11**, 114 (2016).
- [17] M. K. Schmidt, R. Esteban, A. Gonzalez-Tudela, G. Giedke, and J. Aizpurua, "Quantum mechanical description of Raman scattering from molecules in plasmonic cavities," *ACS Nano.* **10**, 6291 (2016).
- [18] J. Liu and K. D. Zhu, "Coupled quantum molecular cavity optomechanics with surface plasmon enhancement," *Photonics Res.* **5**, 450 (2017).
- [19] S. M. Ashrafi, R. Malekfar, A. R. Bahrampour, and J. Feist, "Optomechanical heat transfer between molecules in a nanoplasmonic cavity," *Phys Rev. A* **100**, 013826 (2019).
- [20] M. K. Dezfouli, R. Gordon, and S. Hughes, "Molecular optomechanics in the anharmonic cavity-QED regime using hybrid metaldielectric cavity modes," *ACS Photonics.* **6**, 1400 (2019).
- [21] Y. Zhang, J. Aizpurua and R. Esteban, "Optomechanical Collective Effects in Surface-Enhanced Raman Scattering from Many Molecules," *ACS Photonics.* (2020).
- [22] J. Liu and K. D. Zhu, "Room temperature optical mass sensor with an artificial molecular structure based on surface plasmon optomechanics," *Photonics Res.* **6**, 867 (2018).
- [23] J. J. Li and K. D. Zhu, "All-optical mass sensing with coupled mechanical resonator systems," *Phys. Rep.* **525**, 223 (2013).
- [24] H.J. Chen and K.D. Zhu, "Graphene-based nanoresonator with applications in optical transistor and mass sensing," *Sensors.* **14**, 16740 (2014).
- [25] M. K. Dezfouli and S. Hughes, "Quantum optics model of surface-enhanced Raman spectroscopy for arbitrarily shaped plasmonic resonators," *ACS Photonics.* **4**, 1245 (2017).
- [26] D. Dzsotjan, B. Rousseaux, H. R. Jauslin, G. C. des Francs, C. Couteau and S. Guerin, "Mode-selective quantization and multimodal effective models for spherically layered systems," *Phys Rev. A* **94**,023818 (2016).
- [27] A. Castellini, H.R. Jauslin, B. Rousseaux, D. Dzsotjan, G.C. des Francs, A. Messina and S. Guérin, "Quantum plasmonics with multi-emitters: application to stimulated Raman adiabatic passage," *EPJD* **72**,1 (2018).
- [28] P. T. Kristensen and S. Hughes, "Modes and mode volumes of leaky optical cavities and plasmonic nanoresonators," *ACS Photonics.* **1**, 2 (2014).
- [29] S. Huang, T. Ming, Y. Lin, X. Ling, Q. Ruan, T. Palacios, J. Wang, M. Dresselhaus and J. Kong, "Ultrasmall Mode Volumes in Plasmonic Cavities of NanoparticleOnMirror Structures," *ACS Photonics.* **12**, 5190 (2016).
- [30] R. Gillen, M. Mohr and J. Maultzsch, "Raman active modes in graphene nanoribbons," *Phys. Status Solidi (B)* **247**, 2941 (2010).
- [31] T. Gruner, and D. G. Welsch, "Green-function approach to the radiation-field quantization for homogeneous and inhomogeneous Kramers-Kronig dielectrics," *Phys. Rev. A* **53**, 1818 (1996).
- [32] H. T. Dung, L. Knoll, and D.-G. Welsch, "Spontaneous decay in the presence of dispersing and absorbing bodies: General theory and application to a spherical cavity," *Phys. Rev. A* **62**, 053804 (2000).
- [33] M. M Behbahani, E. Amooghorban, and A. Mahdifar, "Spontaneous emission and the operation of invisibility cloaks," *Phys. Rev. A* **94**, 013854 (2016).
- [34] F. Kheirandish, M. Amooshahi, and E. Amooghorban, "Electromagnetic field quantization in a nonlinear medium," *AIP* **1**, 416 (2009).
- [35] R. Gillen, M. Mohr and J. Maultzsch, "Symmetry properties of vibrational modes in graphene nanoribbons,"

- Phys. Rev. B **81**, 205426 (2010).
- [36] R. Saito, M. Furukawa, G. Dresselhaus and M. S. Dresselhaus, "Raman spectra of graphene ribbons," *J. Phys: Condensed Matter*. **22**, 334203 (2010).
- [37] D. Yan, K.H. Gu, C. N. Ren, L. Chen and J. H. Wu, "Pump-probe response sensitive to atomic excitation in a hybrid optomechanical system," *J. Phys. B: At. Mol. Opt. Phys.* **51**, 155003 (2018).
- [38] Y. P. Gao, T. J. Wang, C. Cao, S. C. Mi, D. Yang, Y. Zhang, and C. Wang, "Effective mass sensing using optomechanically induced transparency in microresonator system," *IEEE Photonics J.* **9**, 1 (2016).
- [39] R. Esteban, J. Aizpurua, and G. W. Bryant, "Strong coupling of single emitters interacting with phononic infrared antennae," *N. J. Phys.* **16**, 013052 (2014).
- [40] G. C. des Francs, J. Barthes, A. Bouhelier, J. C. Weeber, A. Dereux, A. Cuche, and C. Girard, "Plasmonic Purcell factor and coupling efficiency to surface plasmons. Implications for addressing and controlling optical nanosources," *J. Opt.* **18**, 094005 (2016).
- [41] M. O. Scully and M. S. Zubairy, *Quantum optics*, Cambridge University Press, United Kingdom (1997).
- [42] C. W. Qiu, S. Zouhdi, and A. Razek, "Modified spherical wave functions with anisotropy ratio: Application to the analysis of scattering by multilayered anisotropic shells," *IEEE Trans. antennas Propag.* **55**, 3515 (2007).
- [43] M. Abramowitz and I. Stegun, "Handbook of mathematical functions," Dover Publications, (1972).
- [44] C. F. Bohren, and D. R. Huffman, *Absorption and scattering of light by small particles*, Wiley-Interscience publication, New York (1998).
- [45] G. C. Des Francs, "Molecule non-radiative coupling to a metallic nanosphere: an optical theorem treatment," *Int. J. Mol. Sci.* **10**, 3931 (2009).
- [46] G. C. Des Francs, S. Derom, R. Vincent, A. Bouhelier, and A. Dereux, "Mie plasmons: modes volumes, quality factors, and coupling strengths (purcell factor) to a dipolar emitter," *Int. J. Opt.* (2011).
- [47] L. W. Li, P. S. Kooi, M. S. Leong, and T. S. Yee, "Electromagnetic dyadic Green's function in spherically multilayered media," *IEEE Trans. Microw. Theory Tech.* **42**, 2302 (1994).
- [48] D. Liu, C. Daniels, V. Meunier, A. G. Every, and D. Tomanek, "in plane breathing and shear modes in low dimensional nanostructures," *Carbon*. **157**, 364 (2020).
- [49] J. Zhou, and J. Dong, "Radial breathing-like mode of wide carbon nanoribbon," *Phys Lett. A*. **372**, 7183 (2008).
- [50] G. Kalosakas, N. N. Lathiotakis, and K. Papagelis, "Width Dependent Elastic Properties of Graphene Nanoribbons," *Materials*. **14**, 5042 (2021).
- [51] H. Hiura, and M. V. Lee, A. V. Tyurnina and K. Tsukagoshi, "Liquid phase growth of graphene on silicon carbide," *Carbon*. **50**, 5076(2012).
- [52] J. Hakami, L. Wang and M. S. Zubairy, "Spectral properties of a strongly coupled quantum-dot/metal-nanoparticle system," *Phys. Rev. A* **89**, 053835 (2014).
- [53] C. Van Vlack, P. T. Kristensen and S. Hughes, "Spontaneous emission spectra and quantum light-matter interactions from a strongly coupled quantum dot metal-nanoparticle system," *Phys. Rev. B* **85**, 075303 (2012).
- [54] P. B. Johnson and R. W. Christy, "Optical constants of the noble metals," *Phys. Rev. B* **6**, 4370 (1972).
- [55] J. J. Li and K. D. Zhu, "A scheme for measuring vibrational frequency and coupling strength in a coupled nanomechanical resonator-quantum dot system," *Appl. Phys. Lett.* **94**, 063116 (2009).
- [56] W. He, J. J. Li and K. D. Zhu, "Coupling-rate determination based on radiation-pressure-induced normal mode splitting in cavity optomechanical systems," *Opt. Letts.* **35**, 339-341 (2010).
- [57] C. H. Jun, and K. D. Zhu, "Surface plasmon enhanced sensitive detection for possible signature of majorana fermions via a hybrid semiconductor quantum Dot-Metal nanoparticle system," *Sci. Rep.* **5**, 13518 (2015).
- [58] K. L. Ekinici, Y. T. Yang and M. L. Roukes, "Ultimate limits to inertial mass sensing based upon nanoelectromechanical systems," *J. Appl. Phys.* **95**, 2682 (2004).
- [59] G. Bimonte, "Going beyond PFA: A precise formula for the sphere-plate Casimir force," *EPL* **118**, 20002 (2017).
- [60] S. A. Biehs, and G. S. Agarwal, "Anisotropy enhancement of the Casimir-Polder force between a nanoparticle and graphene," *Phys. Rev. A* **90**, 042510 (2014).